

Simulation Algorithms with Exponential Integration for Time-Domain Analysis of Large-Scale Power Delivery Networks

Hao Zhuang, *Student Member, IEEE*, Wenjian Yu, *Senior Member, IEEE*, Shih-Hung Weng, Ilgweon Kang, *Student Member, IEEE*, Jeng-Hau Lin, Xiang Zhang, *Member, IEEE*, Ryan Coutts, Jingwei Lu, *Member, IEEE*, and Chung-Kuan Cheng, *Fellow, IEEE*

Abstract—In this work, we design an efficient and accurate algorithmic framework using matrix exponentials for time-domain simulation of power delivery network (PDN). Thanks to the explicit exponential time integration scheme with high order approximation of differential equation system, our framework can reuse factorized matrices for adaptive time stepping without loss of accuracy. The key operation of matrix exponential and vector product (MEVP) is computed by proposed efficient rational Krylov subspace method and helps achieve large stepping.

With the enhancing capability of time marching and high-order approximation capability, we design R-MATEX, which outperforms the classical PDN simulation method using trapezoidal formulation with fixed step size (TR-FTS). We also propose a distributed computing framework, DR-MATEX, and highly accelerate the simulation speedup by reducing Krylov subspace generations caused by frequent breakpoints from the side of current sources. By virtue of the superposition property of linear system and scaling invariance property of Krylov subspace, DR-MATEX can divide the whole simulation task into subtasks based on the alignments of breakpoints among current sources. Then, the subtasks are processed in parallel at different computing nodes and summed up at the end of simulation to provide the accurate solutions. The experimental results show R-MATEX and DR-MATEX can achieve $11.4\times$ and $68.0\times$ runtime speedups on average over TR-FTS.

Index Terms—Circuit simulation, power delivery/distribution networks, power grid, time-domain/transient simulation, matrix exponential, Krylov subspace method, parallel processing.

I. INTRODUCTION

MODERN VLSI design verification relies heavily on the analysis of power delivery network (PDN) to estimate power supply noises [2]–[9]. Lowering supply voltages, increasing current densities as well as tight design margins lead us to more accurate large-scale PDN simulation. With

advancing technologies [10]–[15], three dimensional (3D) IC structures, and increasing complexities of system designs, the numbers of chip components are easily more than millions, which make VLSI PDNs huge and simulation tasks time-consuming and computationally challenging. Due to the enormous size of modern designs and long simulation runtime of many cycles, instead of general nonlinear circuit simulation [16], [17], PDN is often modeled as a large-scale linear circuit with voltage supplies and time-varying current sources [18]–[20]. Those linear matrices are obtained by parasitic extraction process [5], [21]–[24]. After those processes, we need time-domain large-scale linear circuit simulation to obtain the transient behavior of PDN with above inputs.

Traditional methods in linear circuit simulation solve differential algebra equations (DAE) numerically in explicit ways, e.g., forward Euler (FE), or implicit ways, e.g., backward Euler (BE) and trapezoidal (TR), which are based on low order polynomial approximations for DAEs [25]. Due to the stiffness of systems, which comes from a wide range of time constants of a circuit, the explicit methods require small time step sizes to ensure the stability. In contrast, implicit methods can handle this problem with relative large time steps because of their larger stability regions. However, at each time step, these methods have to solve a linear system, which is sparse and often ill-conditioned. Due to the requirement of a robust solution, compared to iterative methods [26], direct methods [27] are often favored for VLSI circuit simulation, and thus adopted by state-of-the-art power grid (PG) solvers in TAU PG simulation contest [28]–[30]. During transient simulation, only one matrix factorization (LU or Cholesky factorization) is required at the beginning. Then, at each fixed time step, the following transient computation requires only pairs of backward and forward substitutions, which achieves better efficiency over adaptive stepping methods by reusing the factorization matrix [20], [28], [30]. The maximum of time step size is limited by the smallest distances h_{upper} among the breakpoints [31]. Some engineering efforts are spent to break this limitation by sacrificing the accuracy. However, in our paper, we always obey the upper limit h_{upper} of time step to maintain the fidelity of model, which means the fixed time step h cannot go beyond h_{upper} in case of missing breakpoints.

Beyond traditional methods, a class of methods called matrix exponential time integration has been embraced by MEXP [32]. The major complexity is caused by matrix exponen-

Manuscript received in 2015. Corresponding authors: Hao Zhuang (hao.zhuang@cs.ucsd.edu) and Chung-Kuan Cheng (ckcheng@ucsd.edu).

Hao Zhuang, Ilgweon Kang, Jeng-Hau Lin, and Chung-Kuan Cheng are with the Department of Computer Science and Engineering, University of California, San Diego, CA. hao.zhuang@cs.ucsd.edu, jel252@ucsd.edu, igkang@ucsd.edu, ckcheng@ucsd.edu

Wenjian Yu is with the Department of Computer Science and Technology, Tsinghua University, Beijing, China. yu-wj@tsinghua.edu.cn

Shih-Hung Weng was with the Department of Computer Science and Engineering, University of California, San Diego, CA. s2weng@ucsd.edu

Xiang Zhang and Ryan Coutts are with Department of Electrical and Computer Engineering, University of California, San Diego, CA. xiz110@eng.ucsd.edu, rmcoutts@eng.ucsd.edu

Jingwei Lu was with the Department of Computer Science and Engineering, University of California, San Diego, CA. jlu@cs.ucsd.com

tial computations. MEXP utilizes standard Krylov subspace method based on [33] to approximate matrix exponential and vector product. MEXP can solve the DAEs with much higher order polynomial approximations [32], [33] than traditional ones. Another merit of using MEXP-like SPICE simulation for linear circuit is the adaptive time stepping, which can proceed without re-factorizing matrices on-the-fly, while the traditional counterparts cannot avoid such time-consuming process during the adaptive time marching. Nevertheless, when simulating stiff circuits, utilizing standard Krylov subspace method requires large dimension of basis in order to preserve the accuracy of MEXP approximation. It may pose memory bottleneck and degrade the adaptive stepping performance of MEXP.

Nowadays, the emerging multi-core and many-core platforms bring powerful computing resources and opportunities for parallel computing. Even more, cloud computing techniques [34] drive distributed systems scaling to thousands of computing nodes [35]–[37], etc. Distributed computing systems have been incorporated into products of many leading EDA companies and in-house simulators [38]–[42]. However, building scalable and efficient distributed algorithmic framework for transient linear circuit simulation framework is still a challenge to leverage these powerful computing tools.

In this work, we develop a transient simulation framework using matrix exponential integration scheme, *MATEX*, for PDN simulation. Some challenges are required to solve for the efficiency. First, the standard Krylov subspace has convergence problem when the circuit is stiff. Therefore, MEVP is slow by using standard Krylov subspace method. Second, with the capability of large time stepping, we encounter the problem of frequent time breakpoints from current sources of PDN modeling, which triggers the generations of Krylov subspace, even for small time stepping. We have gain when *MATEX* can leverage large time stepping, but waste computational operations for small time step. Our contributions are listed as below:

- MEVP in *MATEX* is computed by rational and invert Krylov subspace methods. Compared to the commonly adopted framework using TR method with fixed time step, our proposed *MATEX* leverages its flexible adaptive (large) time stepping and is still capable of reusing factorized matrix at the beginning of transient simulation.
- Among different Krylov subspace methods, we find rational Krylov subspace is the best strategy for MEVP for PDN simulation. Based on it, we design R-*MATEX* and achieve $11.4\times$ runtime speedup on average against the benchmarks over the traditional method TR-FTS without loss of accuracy.
- DR-*MATEX* is designed to improve *MATEX* with distributed computing resources. First, the PDN's input sources are partitioned into groups based on their alignments. They are assigned to different computing nodes to run the corresponding PDN transient simulations. Then, the results among nodes are summed up, according to the well-known superposition property of linear system. This partition reduces the chances of generating Krylov subspaces and enlarges the time periods of reusing them

during the transient simulation at each node, which brings huge computational advantage and achieves $68.0\times$ speedup over traditional method TR-FTS.

The remainder is organized as follows. Sec. II introduces the background of linear circuit simulation and matrix exponential formulations. Sec. III illustrates the techniques invert and rational Krylov subspace methods to accelerate matrix exponential and vector product computation. Sec. IV presents *MATEX* circuit solver and the distributed framework DR-*MATEX*. Sec. V shows numerical results and Sec. VI concludes this paper.

II. BACKGROUND

A. Transient Simulation of Linear Circuit

Transient simulation of linear circuit is the foundation of PDN simulation. It is formulated as DAEs via modified nodal analysis (MNA),

$$\mathbf{C}\dot{\mathbf{x}}(t) = -\mathbf{G}\mathbf{x}(t) + \mathbf{B}\mathbf{u}(t), \quad (1)$$

where \mathbf{C} is the matrix resulting from capacitive and inductive elements. \mathbf{G} is the conductive matrix, and \mathbf{B} is the input selector matrix. $\mathbf{x}(t)$ is the vector of time-varying node voltages and branch currents. $\mathbf{u}(t)$ is the vector of supply voltage and current sources. In PDN, such current sources are often characterized as pulse or piecewise-linear inputs [18], [20] to represent the activities under the networks. To solve Eq. (1) numerically, it is discretized with time step h and transformed to a linear algebraic system. Given an initial condition $\mathbf{x}(0)$ from DC analysis or previous time step $\mathbf{x}(t)$ and a time step h , $\mathbf{x}(t+h)$ can be obtained by traditional *low order approximation* methods [25].

B. Traditional Low Order Time Integration Schemes

1) *BE*: Backward Euler time integration scheme, a robust implicit first-order method.

$$\left(\frac{\mathbf{C}}{h} + \mathbf{G}\right)\mathbf{x}(t+h) = \frac{\mathbf{C}}{h}\mathbf{x}(t) + \mathbf{B}\mathbf{u}(t+h). \quad (2)$$

2) *TR*: Trapezoidal time integration scheme, a popular implicit second-order method.

$$\begin{aligned} \left(\frac{\mathbf{C}}{h} + \frac{\mathbf{G}}{2}\right)\mathbf{x}(t+h) &= \left(\frac{\mathbf{C}}{h} - \frac{\mathbf{G}}{2}\right)\mathbf{x}(t) \\ &+ \mathbf{B}\frac{\mathbf{u}(t) + \mathbf{u}(t+h)}{2}. \end{aligned} \quad (3)$$

It is probably the most commonly used strategy for large-scale circuit simulation for higher accuracy than BE.

3) *BE-FTS and TR-FTS*: BE and TR with fixed time step (FTS) h are efficient framework and adopted by the top PG solvers in 2012 TAU PG simulation contest [20], [28]–[30]. If only one h is used along the whole simulation, the choice is limited by the minimum distance h_{upper} among all the events of input change (breakpoints [31]). Fig. 1 (a) has $10ps$ as the upper limit for h in BE-FTS and TR-FTS. When the alignments of inputs change (as shown in Fig. 1 (b)), the resulting upper limit for h is $5ps$ for BE-FTS and TR-FTS. If h is larger than the limit, there is no way to guarantee the accuracy since it breaks the fundamental equation, such as Eq. (2) and Eq. (3).

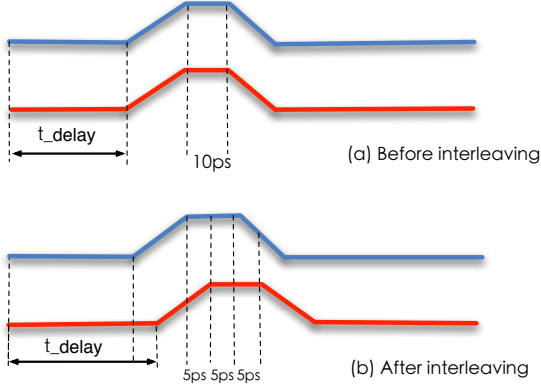


Fig. 1. Example: interleaves two input source to create smaller transition time. (a) Before interleaving, the input sources has smallest transition time $h_{upper} = 10ps$; (b) After interleaving, the input sources has the smallest transition time $h_{upper} = 5ps$.

C. Matrix Exponential Time Integration Scheme

The solution of Eq. (1) can be obtained analytically [25]. For a simple illustration, we convert Eq. (1) into

$$\dot{\mathbf{x}}(t) = \mathbf{A}\mathbf{x}(t) + \mathbf{b}(t), \quad (4)$$

when \mathbf{C} is not singular, $\mathbf{A} = -\mathbf{C}^{-1}\mathbf{G}$ and $\mathbf{b}(t) = \mathbf{C}^{-1}\mathbf{B}\mathbf{u}(t)$. Given the solution at time t and a time step h , the solution at $t+h$ is

$$\mathbf{x}(t+h) = e^{h\mathbf{A}}\mathbf{x}(t) + \int_0^h e^{(h-\tau)\mathbf{A}}\mathbf{b}(t+\tau)d\tau. \quad (5)$$

Assuming that the input $\mathbf{u}(t)$ is piecewise linear (PWL), e.g., $\mathbf{u}(t)$ is linear within every time step, we can integrate the last term of Eq. (5), analytically, turning the solution with matrix exponential operator:

$$\mathbf{x}(t+h) = -\left(\mathbf{A}^{-1}\mathbf{b}(t+h) + \mathbf{A}^{-2}\frac{\mathbf{b}(t+h) - \mathbf{b}(t)}{h}\right) + e^{h\mathbf{A}}\left(\mathbf{x}(t) + \mathbf{A}^{-1}\mathbf{b}(t) + \mathbf{A}^{-2}\frac{\mathbf{b}(t+h) - \mathbf{b}(t)}{h}\right). \quad (6)$$

For the time step choice, breakpoints (also known as input transition spots (TS) [1]) are the time points where slopes of input sources vector change. Therefore, for Eq. (6), the maximum time step starting from t is $(t_s - t)$, where t_s is the smallest one in TS larger than t .

III. KRYLOV SUBSPACE METHODS FOR MATRIX EXPONENTIAL AND VECTOR PRODUCT (MEVP)

Matrix \mathbf{A} in $e^{\mathbf{A}\mathbf{v}}$ is usually above millions, making the direct computation infeasible. The alternative way to compute the product is through Krylov subspace method. In this section, we first introduce the background of standard Krylov subspace for MEVP. Then, we discuss invert (I-MATEX) and rational Krylov subspace (R-MATEX) methods, which highly improve the runtime performance for MEVP.

A. MEXP: MEVP Computation via Standard Krylov Subspace Method

The complexity of $e^{\mathbf{A}\mathbf{v}}$ can be reduced using Krylov subspace method and still maintained in a high order polynomial approximation [33]. MEXP [32] uses standard Krylov subspace, which uses \mathbf{A} when generating basis through Arnoldi process in Alg. 1. First, we reformulate Eq. (6) into

$$\mathbf{x}(t+h) = e^{h\mathbf{A}}(\mathbf{x}(t) + \mathbf{F}(t,h)) - \mathbf{P}(t,h). \quad (7)$$

where

$$\mathbf{F}(t,h) = \mathbf{A}^{-1}\mathbf{b}(t) + \mathbf{A}^{-2}\frac{\mathbf{b}(t+h) - \mathbf{b}(t)}{h} \quad (8)$$

and

$$\mathbf{P}(t,h) = \mathbf{A}^{-1}\mathbf{b}(t+h) + \mathbf{A}^{-2}\frac{\mathbf{b}(t+h) - \mathbf{b}(t)}{h}. \quad (9)$$

The standard Krylov subspace

$$\mathcal{K}_m(\mathbf{A}, \mathbf{v}) := \text{span}\{\mathbf{v}, \mathbf{A}\mathbf{v}, \dots, \mathbf{A}^{m-1}\mathbf{v}\}. \quad (10)$$

obtained by Arnoldi process has the relation

$$\mathbf{A}\bar{\mathbf{V}}_m = \bar{\mathbf{V}}_m\bar{\mathbf{H}}_m + \bar{h}_{m+1,m}\bar{\mathbf{v}}_{m+1}\mathbf{e}_m^T, \quad (11)$$

where $\bar{h}_{m+1,m}$ is the $(m+1, m)$ entry of Hessenberg matrix $\bar{\mathbf{H}}_m$. MEVP is computed via

$$e^{h\mathbf{A}}\mathbf{v} \approx \beta\bar{\mathbf{V}}_m e^{h\bar{\mathbf{H}}_m}\mathbf{e}_1. \quad (12)$$

$\bar{\mathbf{H}}_m$ is usually much smaller compared to \mathbf{A} . The posterior error term is

$$\bar{r}_m(h) = \left| \beta\bar{h}_{m+1,m}\mathbf{e}^T e^{h\bar{\mathbf{H}}_m}\mathbf{e}_1 \right| \quad (13)$$

where $\beta = \|\mathbf{v}\|$. However, in circuit simulation, we consider the residual of $(\mathbf{C}\dot{\mathbf{x}}(t) + \mathbf{G}\mathbf{x}(t))$, instead of $\dot{\mathbf{x}}(t) - \mathbf{A}\mathbf{x}(t)$, which leads to

$$\bar{r}(m,h) = \left| \beta\mathbf{C}\bar{h}_{m+1,m}\mathbf{e}^T e^{h\bar{\mathbf{H}}_m}\mathbf{e}_1 \right| \quad (14)$$

By doing so, it mitigates the overestimation of error bound, especially for the singular \mathbf{C} system.

To generate $\mathbf{x}(t+h)$ by Alg. 1, we use $[\mathbf{L}, \mathbf{U}] = \text{LU_Decompose}(\mathbf{X}_1)$, where, for standard Krylov subspace, $\mathbf{X}_1 = \mathbf{C}$, and $\mathbf{X}_2 = \mathbf{G}$ as inputs. In the line 16 of Alg. 1, $\mathbf{H}_m = \bar{\mathbf{H}}_m$. The error budget ϵ and Eq. (13) are used to determine the convergence condition in current time step h with an order j of Krylov subspace dimension for $e^{\mathbf{A}\mathbf{v}}$ approximation (from line 11 to line 14 in Alg. 1).

The standard Krylov subspace may not be computationally efficient when simulating stiff circuits based on MEXP[32], [43]. For the accuracy of approximation of $e^{\mathbf{A}\mathbf{v}}$, large dimension of Krylov subspace basis is required, which not only brings the computational complexity but also consumes huge memory.

The reason is that Hessenberg matrix \mathbf{H}_m of standard Krylov subspace tends to approximate the large magnitude eigenvalues of \mathbf{A} [44]. Due to the exponential decay of higher order terms in Taylor's expansion, such components are not the crux of circuit system's behavior [44], [45]. Dealing with stiff circuit, therefore, needs to gather more vectors into subspace basis and increases the size of \mathbf{H}_m to fetch more useful

Algorithm 1: MATEX_Arnoldi

Input: $\mathbf{L}, \mathbf{U}, \mathbf{X}_2, h, t, \mathbf{x}(t), \epsilon, \mathbf{P}(t, h), \mathbf{F}(t, h)$
Output: $\mathbf{x}(t+h), \mathbf{V}_m, \mathbf{H}_m, \mathbf{v}$

```
1  $\mathbf{v} = \mathbf{x}(t) + \mathbf{F}(t, h);$ 
2  $\mathbf{v}_1 = \frac{\mathbf{v}}{\|\mathbf{v}\|};$ 
3 for  $j = 1 : m$  do
4    $\mathbf{w} = \mathbf{U} \setminus (\mathbf{L} \setminus (\mathbf{X}_2 \mathbf{v}_j));$  /* a pair of
   backward & forward substitutions. */
5   for  $i = 1 : j$  do
6      $h_{i,j} = \mathbf{w}^T \mathbf{v}_i;$ 
7      $\mathbf{w} = \mathbf{w} - h_{i,j} \mathbf{v}_i;$ 
8   end
9    $h_{j+1,j} = \|\mathbf{w}\|;$ 
10   $\mathbf{v}_{j+1} = \frac{\mathbf{w}}{h_{j+1,j}};$ 
11  if  $r(j, h) < \epsilon$  then
12     $m = j;$ 
13    break;
14  end
15 end
16  $\mathbf{x}(t+h) = \|\mathbf{v}\| \mathbf{V}_m e^{h\mathbf{H}_m} \mathbf{e}_1 - \mathbf{P}(t, h);$ 
```

components, which results in both memory overhead and computational complexity into Krylov subspace generations during time stepping. In the following subsections, we adopt the idea from *spectral transformation* [44], [45] to effectively capture small magnitude eigenvalues in \mathbf{A} , leading to a fast yet accurate MEVP computation.

B. I-MATEX: MEVP Computation via Invert Krylov Subspace Method

Instead of \mathbf{A} , we use \mathbf{A}^{-1} (or $\mathbf{G}^{-1}\mathbf{C}$) as our target matrix to form

$$\mathbf{K}_m(\mathbf{A}^{-1}, \mathbf{v}) := \text{span}\{\mathbf{v}, \mathbf{A}^{-1}\mathbf{v}, \dots, \mathbf{A}^{-(m-1)}\mathbf{v}\}. \quad (15)$$

Intuitively, by inverting \mathbf{A} , the small magnitude eigenvalues become the large ones of \mathbf{A}^{-1} . The resulting \mathbf{H}'_m is likely to capture these eigenvalues first. Based on Arnoldi algorithm, the inverted Krylov subspace has the relation

$$\mathbf{A}^{-1}\mathbf{V}'_m = \mathbf{V}_m \mathbf{H}'_m + h'_{m+1,m} \mathbf{v}'_{m+1} \mathbf{e}_m^T. \quad (16)$$

The matrix exponential $e^{\mathbf{A}\mathbf{v}}$ is calculated as

$$e^{\mathbf{A}\mathbf{v}} = \beta \mathbf{V}'_m e^{h\mathbf{H}'_m} \mathbf{e}_1. \quad (17)$$

To put this method into Alg. 1, it is just by modifying the input variables, $\mathbf{X}_1 = \mathbf{G}$ for the LU decomposition, and $\mathbf{X}_2 = \mathbf{C}$. In the line 16 of Alg. 1, $\mathbf{H}_m = \mathbf{H}'_m{}^{-1}$. The posterior error approximation [1] is

$$r'_m(h) = \left| \beta \mathbf{A} h'_{m+1,m} \mathbf{v}'_{m+1} \mathbf{e}_m^T \mathbf{H}'_m{}^{-1} e^{h\mathbf{H}'_m} \mathbf{e}_1 \right|. \quad (18)$$

which is derived from residual-based error approximation in [45]. However, as mentioned in Sec. III-A, we consider the residual of $(\mathbf{C}\dot{\mathbf{x}}(t) + \mathbf{G}\mathbf{x}(t))$, instead of $(\dot{\mathbf{x}}(t) - \mathbf{A}\mathbf{x}(t))$, which leads to

$$r(m, h) = \left| \beta \mathbf{G} h'_{m+1,m} \mathbf{v}'_{m+1} \mathbf{e}_m^T \mathbf{H}'_m{}^{-1} e^{h\mathbf{H}'_m} \mathbf{e}_1 \right|. \quad (19)$$

We use Eq. (19) at the line 11 of Alg. 1, which is $r(j, h) = r'(j, h)$.

C. R-MATEX: MEVP Computation via Rational Krylov Subspace Method

The shift-and-invert Krylov subspace basis [44] is designed to confine the spectrum of \mathbf{A} . Then, we generate Krylov subspace via

$$\mathbf{K}_m((\mathbf{I} - \gamma\mathbf{A})^{-1}, \mathbf{v}) := \text{span}\{\mathbf{v}, (\mathbf{I} - \gamma\mathbf{A})^{-1}\mathbf{v}, \dots, (\mathbf{I} - \gamma\mathbf{A})^{-(m-1)}\mathbf{v}\}, \quad (20)$$

where γ is a predefined parameter. With this shift, all the eigenvalues' magnitudes are larger than one. Then the invert limits the magnitudes smaller than one. According to [44], [45], the shift-and-invert basis for matrix exponential-based transient simulation is not very sensitive to γ , once it is set to around the order near time steps used in transient simulation. The similar idea has been applied to simple power grid simulation with matrix exponential method [46]. Here, we generalize this technique and integrate into MATEX. The Arnoldi process constructs \mathbf{V}_m and \mathbf{H}_m , and the relationship is given by

$$(\mathbf{I} - \gamma\mathbf{A})^{-1}\tilde{\mathbf{V}}_m = \tilde{\mathbf{V}}_m \tilde{\mathbf{H}}_m + \tilde{h}_{m+1,m} \tilde{\mathbf{v}}_{m+1} \mathbf{e}_m^T. \quad (21)$$

We can project the $e^{\mathbf{A}}$ onto the rational Krylov subspace as follows.

$$e^{\mathbf{A}h}\mathbf{v} \approx \beta \tilde{\mathbf{V}}_m e^{h\frac{\mathbf{I} - \tilde{\mathbf{H}}_m^{-1}}{\gamma}} \mathbf{e}_1. \quad (22)$$

In the line 16 of Alg. 1, $\mathbf{H}_m = \frac{\mathbf{I} - \tilde{\mathbf{H}}_m^{-1}}{\gamma}$. Following the same procedure [1], [45], the posterior error approximation is derived as

$$\tilde{r}_m(h) = \left| \frac{\mathbf{I} - \gamma\mathbf{A}_m}{\gamma} \beta \tilde{h}_{m+1,m} \tilde{\mathbf{v}}_{m+1} \mathbf{e}_m^T \tilde{\mathbf{H}}_m^{-1} e^{h\tilde{\mathbf{H}}_m} \mathbf{e}_1 \right|. \quad (23)$$

Note that in practice, instead of computing $(\mathbf{I} - \gamma\mathbf{A})^{-1}$ directly, $(\mathbf{C} + \gamma\mathbf{G})^{-1}\mathbf{C}$ is utilized. The corresponding Arnoldi process shares the same skeleton of Alg. 1 and Alg. 3 with input matrices $\mathbf{X}_1 = (\mathbf{C} + \gamma\mathbf{G})$ for the LU decomposition, and $\mathbf{X}_2 = \mathbf{C}$. The residual of $(\mathbf{C}\dot{\mathbf{x}}(t) + \mathbf{G}\mathbf{x}(t))$ leads to

$$\tilde{r}(m, h) = \left| \frac{\mathbf{C} + \gamma\mathbf{G}}{\gamma} \beta \tilde{h}_{m+1,m} \tilde{\mathbf{v}}_{m+1} \mathbf{e}_m^T \tilde{\mathbf{H}}_m^{-1} e^{h\tilde{\mathbf{H}}_m} \mathbf{e}_1 \right|. \quad (24)$$

Then, we plug Eq. (24) into the line 11 of Alg. 1, which is $r(j, h) = \tilde{r}(j, h)$.

D. Regularization-Free MEVP Computation

When dealing singular \mathbf{C} , MEXP needs the regularization process [47] to remove the singularity of DAE in Eq.(1). It is because MEXP requires to factorize \mathbf{C} in Alg. 1. This brings extra computational overhead when the case is large. It is not necessary if we can obtain the generalized eigenvalues and corresponding eigenvectors for matrix pencil $(-\mathbf{G}, \mathbf{C})$. Based on [48], we derive the following lemma,

Lemma 1: Considering a homogeneous system $\mathbf{C}\dot{\mathbf{x}} = -\mathbf{G}\mathbf{x}$, \mathbf{u} and λ are the eigenvector and eigenvalue of matrix pencil $(-\mathbf{G}, \mathbf{C})$, then $\mathbf{x} = e^{t\lambda}\mathbf{u}$ is a solution of the system.

I-MATEX and R-MATEX are regularization-free, because we do not need to compute \mathbf{C}^{-1} explicitly during Krylov subspace generation. Instead, we factorize \mathbf{G} for inverted Krylov subspace basis generation (I-MATEX), or $(\mathbf{C} + \gamma\mathbf{G})$ for rational Krylov basis (R-MATEX). Besides, \mathbf{H}'_m and \mathbf{H}_m are invertible, which contain corresponding important generalized eigenvalues/eigenvectors from matrix pencil $(-\mathbf{G}, \mathbf{C})$, and define the behavior of linear dynamic system in Eq. (1).

E. Comparisons among Different Krylov Subspace Algorithms for MEVP Computation

In order to observe the error distribution versus dimensions of standard, invert, and rational Krylov subspace methods for MEVP, we construct a RC circuit with stiffness $\frac{Re(\lambda_{min})}{Re(\lambda_{max})} = 4.7 \times 10^6$, where $\lambda_{max} = -8.49 \times 10^{10}$ and $\lambda_{min} = -3.98 \times 10^{17}$ are the maximum and minimum eigenvalues of $\mathbf{A} = -\mathbf{C}^{-1}\mathbf{G}$. Fig. 2 shows the relative error reductions along the increasing Krylov subspace dimension. The error reduction rate of rational Krylov subspace is the best, while the one of standard Krylov subspace requires huge dimension to capture the same level of error. For example, it costs almost $10\times$ to achieve around relative error 1% compared to invert and rational Krylov subspace. The relative error $\|e^{h\mathbf{A}\mathbf{v}} - \beta\mathbf{V}_m e^{h\mathbf{H}_m}\mathbf{e}_1\|/\|e^{h\mathbf{A}\mathbf{v}}\|$, where $h = 0.4ps$, $\gamma = 10^{-13}$. \mathbf{A} is a relatively small matrix and computed by MATLAB *expm* function; Therefore, $e^{h\mathbf{A}\mathbf{v}}$ serves as the baseline for accuracy. The relative error is the real relative difference compared to the analytical solution $e^{h\mathbf{A}\mathbf{v}}$ of the ODE $\frac{dx}{dt} = \mathbf{A}x$ with an initial vector \mathbf{v} , which is generated by MATLAB *rand* function.

The error reduction rate of standard Krylov subspace is worst, while the one of rational Krylov subspace is the best. It is the reason that we prefer rational Krylov subspace (R-MATEX). The relative errors of BE, TR and FE are 0.0594, 0.4628, and 2.0701×10^4 , respectively. The large error of FE is due to the instability issue of its low order explicit time integration scheme. We change the entries in \mathbf{C} and \mathbf{G} with stiffness 4.7×10^{10} . In Fig. 2, when $m = 3$, standard, invert and rational Krylov subspace methods have 0.8465, 0.0175, and 0.0065, respectively. It illustrates the power of matrix exponential method. Our proposed methods are all stable and can achieve improved error numbers. Fig. 3 illustrates the stable reduction rate of rational method. Both invert and rational Krylov subspace methods are good candidates for stiff circuit system.

Regarding the relative error distributions vs. time step h and dimension m , Fig. 4, Fig. 5, and Fig. 6 are computed by standard, invert, and rational Krylov subspaces ($\gamma = 5 \times 10^{-13}$), respectively. Fig. 4 shows the flat region of high error distribution along the time step range of interest, while the small ('unrealistic') time step the method has very small error. Compared to Fig. 4, invert (Fig. 5) and rational (Fig. 6) Krylov subspace methods reduce errors quickly for large h , which is useful to simulation. It is because the larger step, the more dominating role first smallest magnitude eigenvalues play, which are well captured by rational Krylov subspace-based method [44].

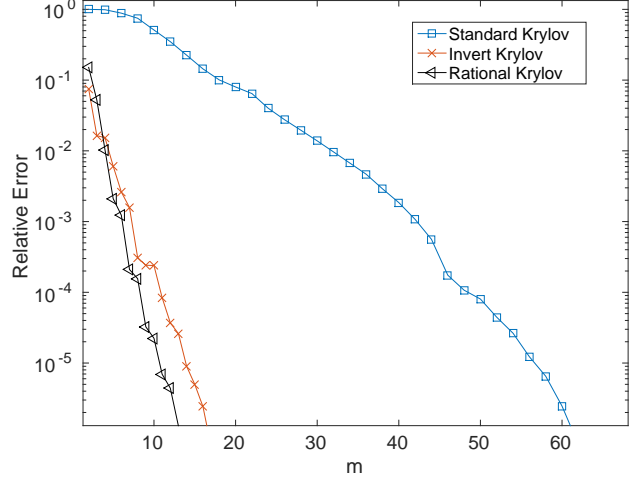


Fig. 2. The relative error vs. dimensional m of different Krylov subspace method. The relative error $\|e^{h\mathbf{A}\mathbf{v}} - \beta\mathbf{V}_m e^{h\mathbf{H}_m}\mathbf{e}_1\|/\|e^{h\mathbf{A}\mathbf{v}}\|$, where $h = 0.4ps$, $\gamma = 10^{-13}$. Note: the relative error is the real relative difference compared to analytical solution $e^{h\mathbf{A}\mathbf{v}}$ of the ODE $\frac{dx}{dt} = \mathbf{A}x$ with an initial vector \mathbf{v} , which is generated by MATLAB *rand* function and its entries are positive numbers in $(0, 1]$. The error reduction rate of standard Krylov subspace is the worst. The error reduction rate of rational Krylov subspace is the best. It is the reason we prefer rational Krylov subspace (R-MATEX). The relative errors 0.0594 for BE, 0.4628 for TR, and 2.0701×10^4 for FE, which is due to the instability issue of FE's low order explicit time integration scheme. When $m = 3$, standard, invert and rational Krylov subspace methods have 0.8465, 0.0175, and 0.0065, respectively. Our methods are all stable and can achieve better error numbers.

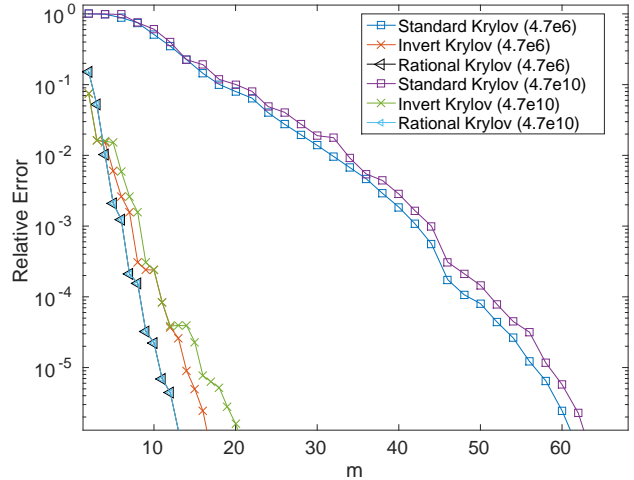


Fig. 3. The relative error vs. dimension m of different Krylov subspace method. The relative error $\|e^{h\mathbf{A}\mathbf{v}} - \beta\mathbf{V}_m e^{h\mathbf{H}_m}\mathbf{e}_1\|/\|e^{h\mathbf{A}\mathbf{v}}\|$, where $h = 0.4ps$, $\gamma = 10^{-13}$. The rational Krylov subspace has very stable error reduction rate. The stiffness degrades the performance of standard Krylov subspace method. The number in the bracket represents the stiffness of the system.

The error of rational Krylov subspace is insensitive to γ when it is selected between the time-step range of interests (Fig. 7). Above all, rational Krylov (R-MATEX) and invert Krylov (I-MATEX) subspace methods have much greater performance than standard version. When we deal with more stiff cases, standard Krylov subspace is not a feasible choice

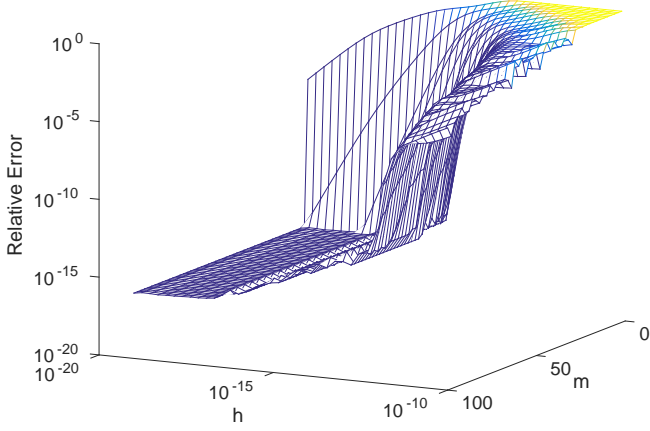


Fig. 4. $\|e^{h\mathbf{A}\mathbf{v}} - \beta\tilde{\mathbf{V}}_m e^{h\tilde{\mathbf{H}}_m}\| / \|e^{h\mathbf{A}\mathbf{v}}\|$ vs. time step h and dimension of standard Krylov subspace basis (m). The standard Krylov subspace approximate well in extremely small h , since it captures the important eigenvalues of \mathbf{A} at that region. However, the small h is not useful to simulation. For large h , it costs large amount of m to reduce the error.

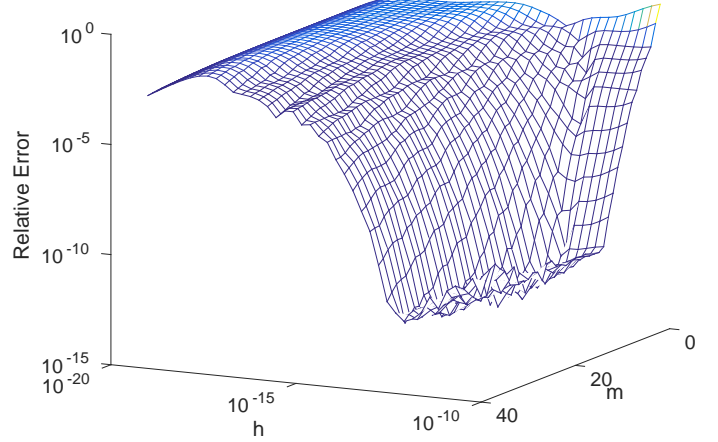


Fig. 6. $\|e^{h\mathbf{A}\mathbf{v}} - \beta\tilde{\mathbf{V}}_m e^{h\frac{\mathbf{I} - \tilde{\mathbf{H}}_m^{-1}}{\gamma}} \mathbf{e}_1\| / \|e^{h\mathbf{A}\mathbf{v}}\|$, where $\gamma = 5 \times 10^{-13}$, vs. time step h and dimension of rational Krylov subspace basis (m). Compared to Fig. 4, rational Krylov subspace method reduces the errors for large h as Fig. 5.

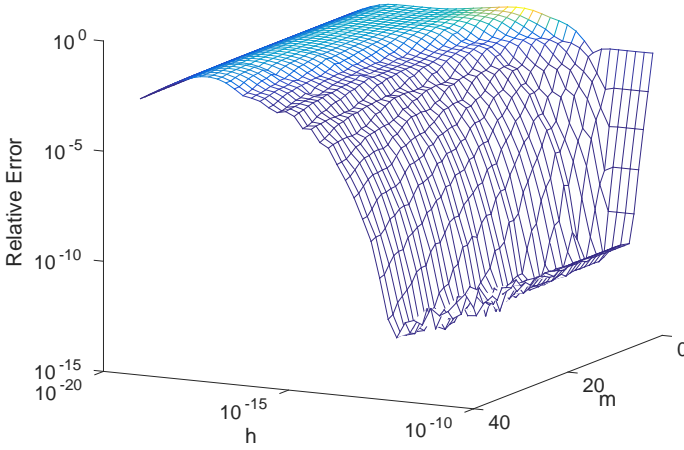


Fig. 5. $\|e^{h\mathbf{A}\mathbf{v}} - \beta\mathbf{V}'_m e^{h\mathbf{H}'_m^{-1}}\| / \|e^{h\mathbf{A}\mathbf{v}}\|$ vs. time step h and dimension of invert Krylov subspace basis (m). Compared to Fig. 4, invert Krylov subspace method reduces the errors for large h .

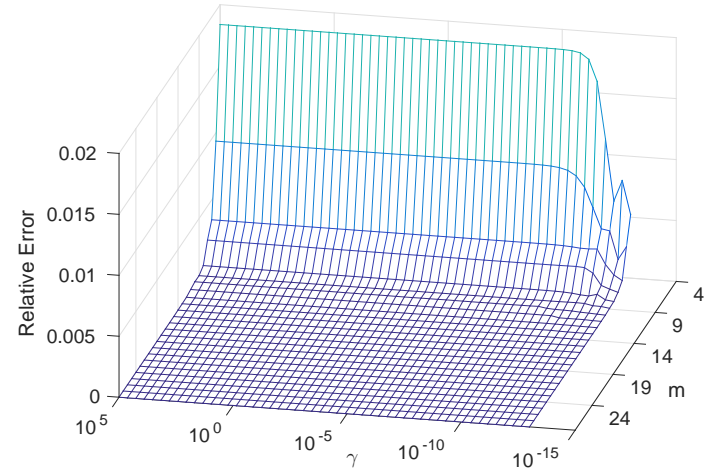


Fig. 7. $\|e^{h\mathbf{A}\mathbf{v}} - \beta\tilde{\mathbf{V}}_m e^{h\frac{\mathbf{I} - \tilde{\mathbf{H}}_m^{-1}}{\gamma}} \mathbf{e}_1\| / \|e^{h\mathbf{A}\mathbf{v}}\|$, where $h = 4ps$. The flat region shows the error actually insensitive what γ chosen in rational Krylov subspace method when γ is in the range of step size h of interests.

due to the large dimension, causing memory consumptions and poor runtime performance, which is shown in Fig. 2 and Fig. 3.

IV. MATEX FRAMEWORK

A. MATEX Circuit Solver

Matrix exponential kernel with Krylov subspace method can solve Eq. (1) with larger time steps and high accuracy than lower order approximation methods. We incorporate matrix exponential integration scheme with Krylov subspace method into our MATEX framework, which is summarized in Alg. 2. Line 1 is to set \mathbf{X}_1 and \mathbf{X}_2 according to the choice of Krylov subspace method.

- I-MATEX: $\mathbf{X}_1 = \mathbf{G}$, $\mathbf{X}_2 = \mathbf{C}$.

- R-MATEX: $\mathbf{X}_1 = \mathbf{C} + \gamma\mathbf{G}$, $\mathbf{X}_2 = \mathbf{C}$.

For linear system of PDN, the line 4 is only performed once, and can be reused in the while loop from the line 5 to 9. It is the same as traditional fixed step low order schemes, BE-FTS or TR-FTS. Line 8 uses Arnoldi process (Alg. 1) with inputs, including factorized \mathbf{L} and \mathbf{U} , to construct Krylov subspace.

B. DR-MATEX (Distributed R-MATEX Framework): Accelerated Simulation by Decomposing the Groups of Current Sources and Distributed/Parallel Processing.

With the ability of large step marching, the input term \mathbf{b} embedded in Eq. (5) actually serves a double-edged sword in MEVP computation. There are usually many input currents in PDNs as well as their breakpoints, which narrow the

Algorithm 2: MATEX Circuit Solver

Input: $\mathbf{C}, \mathbf{G}, \mathbf{B}, \mathbf{u}(t), \tau, \epsilon, \gamma$ error tolerance E_{tol} , and simulation time T

Output: \mathbf{x} from $[0, T]$

```
1 Set  $\mathbf{X}_1, \mathbf{X}_2$ ; /* R-MATEX:  $\mathbf{X}_1 = \mathbf{C} + \gamma\mathbf{G}$ ,  
    $\mathbf{X}_2 = \mathbf{C}$ ; or I-MATEX:  $\mathbf{X}_1 = \mathbf{G}$ ,  $\mathbf{X}_2 = \mathbf{C}$ . */  
2  $t = 0$ ;  
3  $\mathbf{x}(t) = \text{DC\_analysis}$ ;  
4  $[\mathbf{L}, \mathbf{U}] = \text{LU\_Decompose}(\mathbf{X}_1)$ ;  
5 while  $t < T$  do  
6   Compute maximum allowed step size  $h$ ;  
7   Update  $\mathbf{P}(t, h), \mathbf{F}(t, h)$ ;  
8   Obtain  $\mathbf{x}(t+h)$  by Algorithm 1 with inputs  
    $[\mathbf{L}, \mathbf{U}, \mathbf{X}_2, h, t, \mathbf{x}(t), \epsilon, \mathbf{P}(t, h), \mathbf{F}(t, h)]$ ;  
9    $t = t + h$ ;  
10 end
```

regions for the time stepping of matrix exponential-based method due to the unaligned breakpoints. The region before the next transition t_s may be shortened when there are a lot of independent input sources injected into the linear system. It leads to more chances of generating new Krylov subspace. We want to reduce the number of Krylov subspace generations to improve the runtime performance. (This is also true for the low order integration schemes, but the capability of efficient time stepping and theoretical limitations of low order accuracy refrain them from seeing the possible improvement space.)

Note the flexible time stepping can choose any time spot until the next input transition spot t_s , as long as the approximation of $e^{\mathbf{A}\mathbf{v}}$ is accurate enough. The Krylov subspace can be reused when $t+h \in [t, t_s]$, only by scaling \mathbf{H}_m with h in $\mathbf{x}(t+h) = \|\mathbf{v}\| \mathbf{V}_m e^{h\mathbf{H}_m} \mathbf{e}_1 - \mathbf{P}(t, h)$. This is an important feature that even doing the adaptive time stepping, we can still use the last Krylov subspaces.

Since the PDN is linear dynamical system, we can utilize the well-known superposition property of linear system and distributed computing model to tackle this challenge. To illustrate our distributed version of MATEX framework, we first define three terms for breakpoints of input sources:

- *Local Transition Spot (LTS)*: the set of *TS* at a input source to the PDN.
- *Global Transition Spot (GTS)*: the union of *LTS* among all the input sources to the PDN.
- *Snapshot*: a set $GTS \setminus LTS$ at a input source.

If we simulate the PDN with respective to all the inputs, *GTS* are the places where generations of Krylov subspace cannot be avoided. For example, there are three input sources in a PDN (Fig. 9). The input waveforms are shown in Fig. 10. The first line is *GTS*, which is contributed by the union of *LTS* in input sources #1, #2 and #3.

However, we can partition the task into sub-tasks by simulating each input source individually. Then, each sub-task generates Krylov subspaces based on its own *LTS* and keeps track of *Snapshot* for the later usage of summation via superposition. In addition, the points in *Snapshot* between

two points $l_1, l_2 \in LTS$ ($l_1 < l_2$), can reuse the Krylov subspace generated at l_1 , which is mentioned in Sec. 16. For each node, the chances of Krylov subspaces generations are reduced and the time periods of reusing these subspaces are enlarged locally, which bring huge computational benefit when processing these subtasks in parallel.

Above, we divide the simulation task by input sources. We can, more aggressively, decompose the task according to the “bump” shapes within such input pulse sources. We group the input sources which have the same ($t_{\text{delay}}, t_{\text{rise}}, t_{\text{fall}}, t_{\text{width}}$) into one set, which is shown in Fig. 11. There are four groups in Fig. 11, Group 1 contains *LTS*#1.1, Group 2 contains *LTS*#2.1, Group 3 contains *LTS*#2.2, and Group 4 contains *LTS*#1.2 and #3.

Our proposed framework MATEX is shown in Fig. 8. After pre-computing *GTS* and decomposing *LTS* based on “bump” shape (Fig. 11), we group them and form *LTS* #1 ~ # K (Note: There are alternative decomposition strategies. It is also easy to extend the work to deal with different input waveforms. We try to keep this part as simple as possible to emphasize our framework).

MATEX scheduler sends out *GTS* and *LTS* to different MATEX slave node. Then the simulations are performed in parallel. There are no communications among nodes before the “write back”. Within each slave node, “circuit solver” (Alg. 3) computes transient response with varied time steps. Solutions are obtained without re-factorizing matrix during the transient computing. After finishing all simulations from slave nodes, they writes back the results and informs the MATEX scheduler.

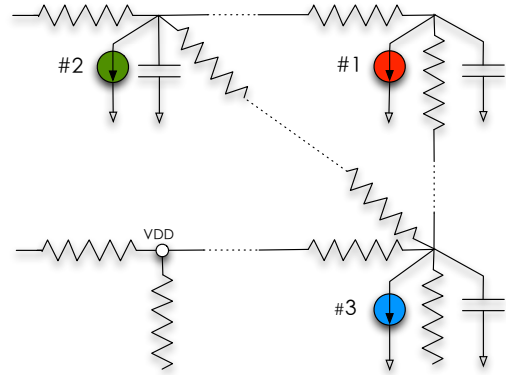


Fig. 9. Part of a PDN model with input sources from Fig. 10.

Complexity Analysis: Suppose on average we have Krylov subspace basis dimension m at each time step along the time span, one pair of backward and forward substitutions has time complexity T_{bs} . The total time complexity of serial parts is T_{serial} , which includes matrix factorizations, local results collection, etc. The matrix exponential evaluation using \mathbf{H}_m is T_H which costs time complexity $O(m^3)$, plus extra T_e to form \mathbf{x} , which costs $O(nm^2)$. Given K points of *GTS*, without decomposition of input transitions, the time complexity is $KmT_{bs} + K(T_H + T_e) + T_{serial}$. After dividing the input transitions and sending to enough computing nodes, we have k points of *LTS* for each node based on feature extraction and grouping (e.g., $k = 4$ for one “bump” shape feature). The total computation complexity is $kmT_{bs} + K(T_H + T_e) +$

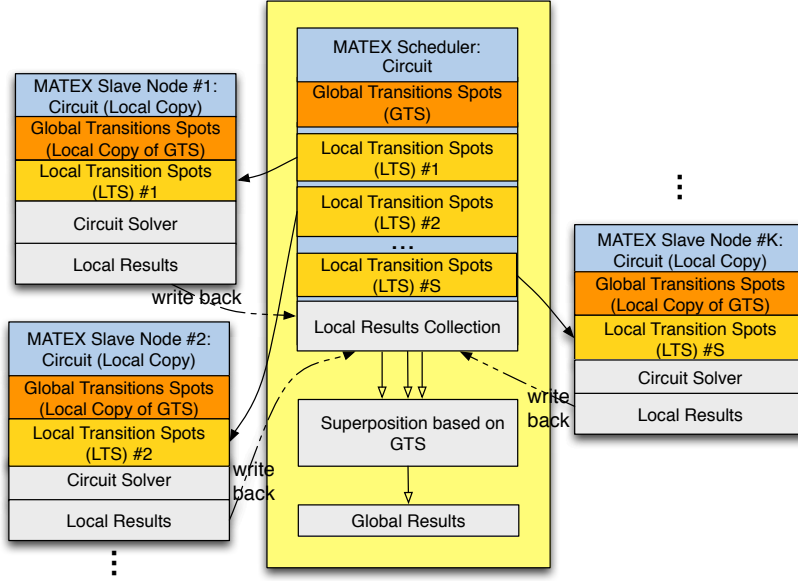


Fig. 8. DR-MATEX: distributed MATEX framework using MATEX circuit solver

Algorithm 3: DR-MATEX: distributed NATEX framework using R-MATEX

Input: $LTS \#k$, GTS , \mathbf{X}_1 , \mathbf{X}_2 , and \mathbf{P}_k , \mathbf{F}_k , which contain the corresponding \mathbf{b} for node k ; error tolerance E_{tol} , and simulation time T .

Output: Local solution \mathbf{x} along GTS in node $k \in [1, \dots, S]$, where S is the number of nodes

```

1  $t = T_{start}$ ;
2  $\mathbf{x}(t) = \text{Local\_Initial\_Solution}$ ;
3  $[\mathbf{L}, \mathbf{U}] = \text{LU\_Decompose}(\mathbf{X}_1)$ ;
4 while  $t \leq T_{end}$  do
5   Compute maximum allowed step size  $h$  based on
    $GTS$ ;
6   if  $t \in LTS \#k$  then
7     /* Generate the Krylov subspace
       for the time point of  $LTS$  and
       compute  $\mathbf{x}$  */
        $[\mathbf{x}(t+h), \mathbf{V}_m, \mathbf{H}_m, \mathbf{v}] =$ 
       MATEX_Arnoldi( $\mathbf{L}, \mathbf{U}, \mathbf{X}_2,$ 
        $h, t, \mathbf{x}(t), \epsilon, \mathbf{P}_k(t, h), \mathbf{F}_k(t, h)$ );
8      $a_{lts} = t$ ;
9   end
10  else
11    /* Compute the  $\mathbf{x}$  at  $Snapshot$  by
    reusing the latest Krylov
    subspace */
     $h_a = t + h - a_{lts}$ ;
12     $\mathbf{x}(t+h) = \|\mathbf{v}\| \mathbf{V}_m e^{h_a \mathbf{H}_m} \mathbf{e}_1 - \mathbf{P}_k(t, h)$ ;
13  end
14   $t = t + h$ ;
15 end

```

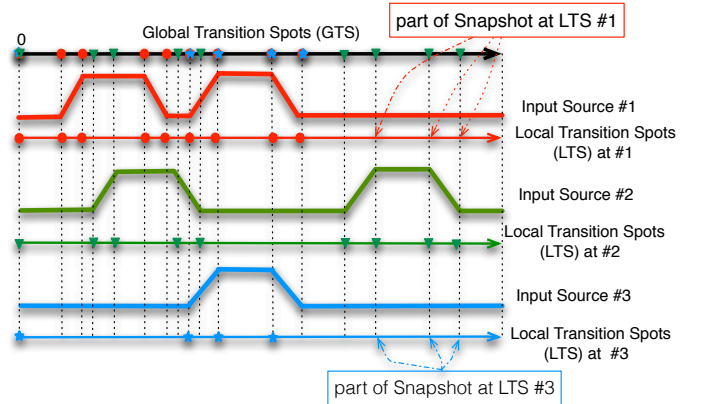


Fig. 10. Illustration of input transitions. GTS: Global Transition Spots; LTS: Local Transition Spots; Snapshots: the crossing positions by dash lines and LTS $\#k$ without solid points.

T_{serial} , where $K(T_H + T_e)$ contains the portion of computing $Snapshot$. The speedup of distributed computing over single MATEX,

$$\text{Speedup} = \frac{KmT_{bs} + K(T_H + T_e) + T_{serial}}{kmT_{bs} + K(T_H + T_e) + T_{serial}}. \quad (25)$$

In R-MATEX, we have very small m . Besides, T_{bs} is larger than $T_H + T_e$. Therefore, the most dominating part is the KmT_{bs} . We can always decompose input transitions, and make k very small compared to K . Traditional method with fixed step size has N steps for the entire simulation. The complexity is $NT_{bs} + T_{serial}$. Then the speedup of distributed MATEX over the ones with fixed step size is,

$$\text{Speedup}' = \frac{NT_{bs} + T_{serial}}{kmT_{bs} + K(T_H + T_e) + T_{serial}}. \quad (26)$$

Usually, N is much larger K and km . Uniform step sizes make N increase due to resolution of input transitions, to

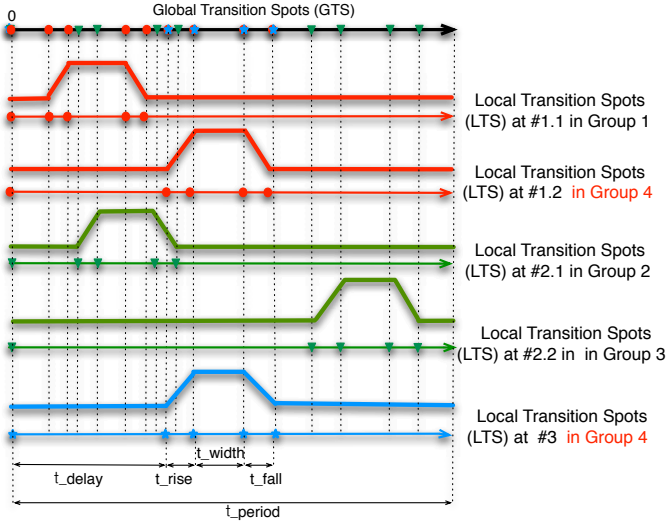


Fig. 11. Grouping of “Bump” shape transitions for sub-task simulation. The matrix exponential-based method can utilize adaptive stepping in each LTS and reuse the Krylov subspace generated at the most recent solid point. However, traditional methods (TR, BE, etc) still need to do time marching step by step, either by pairs of backward and forward substitutions and proceed with fixed time step, or re-factorize matrix and solve linear system when using adaptive stepping. (Pulse input information: t_{delay} : initial delay time; t_{rise} : rise time; t_{width} : width of pulse-wise; t_{fall} : fall time; and t_{period} : period).

which K is not so sensitive. As mentioned before, k can be maintained in a small number. When elongating time span of simulation, N will increase, however, k will not change due to its irrelevance to time span (may bring more input transition features and increase computing nodes), and speedups tend to become larger. Therefore, our MATEX is more robust and has promising theoretical speedups.

V. EXPERIMENTAL RESULTS

We implement all the algorithms in MATLAB R2014b and use UMFPACK package for LU factorization. First, we compare I-MATEX, R-MATEX and TR in order to show our runtime improvements in single machine framework in Table II. Second, we show our distributed framework DR-MATEX achieves very large speedups in Table III. The experiments are conducted on servers with Intel(R) Xeon (R) E5-2640 v3 2.60GHz processor and 125GB memory.

A. Performance of I-MATEX and R-MATEX in Sec. IV-A

We compare our proposed I-MATEX, R-MATEX against the popular TR-FTS using the IBM power grid suite [18]. In the current sources, the smallest interval between two breakpoints is $h_{\text{upper}} = 10ps$, which puts the upper limit of the TR’s step size. All of these cases have very large numbers of input current sources. Table I shows the details of each benchmark circuit of which size ranges from 54K up to 3.2M. The simulation time is $10ns$. From `ibmpg1t` to `ibmpg6t`, TR uses fixed step size in $10ps$. We also change the IBM power grid benchmark to make the the smallest distance among breakpoints $1ps$ by interleaving input sources’ breakpoints (similar as Fig. 1). Therefore, the fixed step size method

TABLE I
SPECIFICATIONS OF IBM POWER GRID SUITE

Design	#R	#C	#L	#I	#V	#Nodes
<code>ibmpg1t</code>	41K	11K	277	11K	14K	54K
<code>ibmpg2t</code>	245K	37K	330	37K	330	165K
<code>ibmpg3t</code>	1.6M	201K	955	201K	955	1.0M
<code>ibmpg4t</code>	1.8M	266K	962	266K	962	1.2M
<code>ibmpg5t</code>	1.6M	473K	277	473K	539K	2.1M
<code>ibmpg6t</code>	2.4M	761K	381	761K	836K	3.2M

can only use at most $1ps$. The names of those benchmarks are `ibmpg1t_new`, `ibmpg2t_new`, `ibmpg3t_new`, `ibmpg4t_new`, `ibmpg5t_new` and `ibmpg6t_new`.

In TR-FTS, we use only one matrix factorization process for transient computing. Actually, multiple factorized matrices can be deployed [49], [50] and choose one of them during the stepping. The problem is the memory overhead and multiple matrix factorizations. Another point is if large time step h^t is chosen, the low order scheme cannot maintain the accuracy.

Experiment is conducted on a single computing node. In Table II, we record the total transient simulation runtime Total(s) after non-numerical computing at the beginning, e.g., parsing the netlist and matrix stamping. We also record “pure transient computing” Tran(s) excluding LU. The speedups of I-MATEX is not as large as R-MATEX because I-MATEX with a large spectrum of \mathbf{A} generates large dimension of Krylov subspace. Meanwhile, the step size is not large enough to let it fully harvest the gains from large time-step marching. On the contrary, R-MATEX needs small number of rational Krylov subspace methods ranging from 2 to 9 in those cases. Therefore, they can benefit from large time stepping, shown as $SPDP_{tr}^r$ and $SPDP_{tr}^{hr}$, respectively. For `ibmpg4t`, R-MATEX achieves maximum speedups resulted from relative small number points of breakpoints around 44 points, while the majority of others have over 140 points. In Table II, our single mode R-MATEX achieves the average speedups of $11.4\times$.

B. Performance of DR-MATEX in Sec. IV-B

We test our distributed DR-MATEX in the following experiments with power grid benchmarks. Distributed framework divides the region at the very beginning. Then stepping can actually benefit from the large time step. These cases have many input transitions (GTS) that limit step sizes of R-MATEX. Exploiting distributed computing, we decompose the input transitions, to obtain much fewer transitions of LTS for computing nodes. The input source numbers are over ten thousand in the benchmarks, however, based on “bump” feature (as shown in Fig. 11), we obtain a fairly small number of the required computing nodes, which is shown as $Group\ \#$ in Table. III. (The hundred machines to process in parallel is quite normal [34], [35].) We pre-compute GTS and LTS groups and assign sub-tasks to corresponding nodes. MATEX scheduler is only responsible for simple superposition calculation at the end of simulation. Since the slave nodes are in charge of all the computing procedures (Fig. 8) for transient simulation, and have no communications with each other during transient simulations, we can easily emulate multiple-node environment using our limited number of servers. We assign one MATLAB

TABLE II
 PERFORMANCE COMPARISONS: TR-FTS, I-MATEX, AND R-MATEX. **DC(s)**: RUNTIME OF DC ANALYSIS (SECONDS); **Tran(s)**: RUNTIME OF TRANSIENT SIMULATION AFTER DC; **Total(s)**: RUNTIME OF OVERALL TRANSIENT SIMULATION; **SPDP _{γ} ^r**: SPEEDUP OF R-MATEX OVER I-MATEX WITH RESPECT TO **Tran(s)**; **SPDP_{tr}^r**: SPEEDUP OF R-MATEX OVER TR-FTS WITH RESPECT TO **Tran(s)**.

Design	DC(s)	TR-FTS		I-MATEX		R-MATEX		Speedups	
		Tran(s)	Total(s)	Tran(s)	Total(s)	Tran(s)	Total(s)	SPDP _{γ} ^r	SPDP _{tr} ^r
ibmpg1t	0.14	5.69	6.00	22.17	22.34	4.22	4.58	6.7×	1.3×
ibmpg2t	0.84	39.95	41.85	98.80	99.91	22.34	24.42	4.8×	1.8×
ibmpg3t	16.41	263.21	295.03	970.32	986.95	189.37	219.06	5.8×	1.4×
ibmpg4t	13.48	460.81	501.87	429.18	454.73	84.45	121.51	5.9×	5.5×
ibmpg5t	9.02	476.61	497.96	2378.96	2392.13	276.27	299.70	10.6×	1.7×
ibmpg6t	15.31	715.97	749.07	3066.21	3084.36	425.25	461.91	9.5×	1.7×
ibmpg1t_new	0.16	51.33	51.66	24.33	24.51	4.88	5.29	6.4×	10.5×
ibmpg2t_new	0.85	431.43	433.46	99.54	100.69	25.45	27.86	4.7×	17.0×
ibmpg3t_new	16.27	3716.49	3749.03	1019.49	1035.63	196.17	225.55	5.8×	18.9×
ibmpg4t_new	18.26	5044.63	5085.33	628.87	658.21	115.63	163.79	6.2×	43.6×
ibmpg5t_new	10.48	5065.89	5110.13	2411.32	2422.96	286.43	313.00	9.9×	17.7×
ibmpg6t_new	13.08	7015.30	7059.69	3781.10	3797.47	456.24	495.23	10.5×	15.4×
Average	—	—	—	—	—	—	—	7.2×	11.4×

instance at each node with single thread computing mode by using “matlab -singleCompThread”. After all slave nodes finish their jobs, we report the maximum runtime among these nodes as the total runtime “Total(s)” of DR-MATEX in Table. III. We also record “pure transient computing” as “Tran(s)”, which is the maximum runtime of the counterparts among all computing nodes.

In the baseline TR-FTS, we have $h = 10ps$, which requires 1,000 pairs of backward and forward substitutions for the transient computing after factorizing $(C/h + G/2)$, for `ibmpg1t~ibmpg6t`; And $h = 1ps$ with 10,000 pairs for `ibmpg1t_new~ibmpg6t_new`. In the circuit solver using R-MATEX within DR-MATEX, $\gamma = 5 \times 10^{-12}$ is set to sit among the order of varied time steps during the simulation (since Sec. III-E discusses the insensitivity of γ around the step size of interests). TR-FTS is not distributed because it has no gain by dividing the current source as we do for the DR-MATEX. TR-FTS cannot avoid the repeated pairs of forward and backward substitutions and such adaptive stepping only degrades the performance.

In Table. III, our distributed mode gains 68.0× speedups on average with respect to the pure transient computing. The average peak dimension m of rational Krylov subspace is 6.7. The memory overhead ratio for each node (around 1.4× over TR-FTS on average) is slightly larger, but it is worthwhile compared to the large runtime improvement. With the huge reduction of runtime on Krylov subspace generations, the serial parts, including LU and DC, play more dominating roles in DR-MATEX, which can be further improved using advance methods, such as [51].

VI. CONCLUSIONS AND FUTURE DIRECTIONS

In this work, we propose an efficient framework MATEX for accurate PDN time-domain simulation by using the exponential integration scheme. In this paper, we visualize the error distributions to show the advantages of using rational (R-MATEX) and invert (I-MATEX) Krylov subspaces for matrix exponential and vector product (MEVP) in large-scale linear circuit simulation over standard Krylov subspace method (MEXP). For the PDN simulation, our time integration scheme

has the capability of adaptive time stepping without repeating matrix factorizations, which cannot be achieved by current traditional PDN simulation methods. Compared to the commonly adopted framework using TR method with fixed time step (TR-FTS), our single mode framework (R-MATEX) gains runtime speedups 11.4× on average. Besides, we also show the distributed MATEX (DR-MATEX) framework leverages the superposition property of linear system and decomposes the task based on the feature of input sources to reduce chances of Krylov subspace generations for each node. We achieve runtime improvement around 68.0× on average by the distributed computing framework.

In this paper, we show the exponential integration scheme with Krylov subspace methods maintains high order accuracy and more flexible time-marching ability, compared to traditional low order scheme methods. The exponential integration framework was actually mentioned by the very early work in circuit simulation algorithms [25], but it had not attracted too much attentions due to the high complexities of computations during that time. Nowadays, thanks to the progress of Krylov subspace based methods, which highly ease the computational problem for matrix exponential based methods, we can enjoy certain features of exponential integration, which are hardly obtained from traditional time integration schemes. For example, exponential integration can also serve as stable explicit schemes [52], [53] for general dynamical systems. It is a promising framework for the future circuit simulation algorithms and software. The opportunities of parallel and distributed computing based on the cutting-edge multi-core and many-core hardware are also worth exploring for the further parallelism.

ACKNOWLEDGMENT

We acknowledge the support from NSF-CCF 1017864. Hao Zhuang also thanks the supports from the Powell Fellowship and the Qualcomm FMA Fellowship. We thank Prof. Alexander Ostermann, Prof. Marlis Hochbruck and Prof. Mike Botchev, Dr. John Loffeld, Prof. Mayya Tokman, Dr. Quan Chen, and Dr. Peng Du.

TABLE III

DR-MATEX PERFORMANCE. **Group #**: GROUP NUMBER OF THE TESTCASES. DIVIDED BY THE FIRST BREAKPOINTS; **Tran(s)**: RUNTIME OF TRANSIENT SIMULATION AFTER DC; **Total(s)**: RUNTIME OF OVERALL TRANSIENT SIMULATION; **Max. and Avg. Diff.**: MAXIMUM AND AVERAGE DIFFERENCES COMPARED TO THE SOLUTIONS OF ALL OUTPUT NODES PROVIDED. **SPDP_r**: SPEEDUP OVER R-MATEX'S **Tran(s)** IN TABLE II. **SPDP_{tr}**: SPEEDUP OVER TR-FTS'S **Tran(s)** IN TABLE II. **Peak m**: THE PEAK DIMENSION USED IN DR-MATEX FOR MEVP; **Mem. Ratio over TR-FTS**: THE PEAK MEMORY COMPARISON BETWEEN THE MAXIMUM MEMORY CONSUMPTION OF DR-MATEX OVER TR-FTS IN TABLE II.

Design	DR-MATEX					Speedups		Peak <i>m</i>	Mem. Ratio over TR-FTS
	Group #	Tran(s)	Total(s)	Max Diff.	Avg Diff.	SPDP _r	SPDP _{tr}		
ibmpg1t	100	0.43	0.82	1.8e-3	6.0e-4	9.8×	13.2×	6	1.1
ibmpg2t	100	1.76	3.80	2.0e-3	4.8e-4	12.7×	22.7×	6	1.3
ibmpg3t	100	17.70	46.64	1.3e-3	3.1e-4	10.7×	14.9×	6	1.4
ibmpg4t	15	31.51	76.81	9.8e-4	2.5e-4	2.7×	14.6×	8	1.4
ibmpg5t	100	35.22	59.34	1.2e-3	2.5e-4	7.8×	13.5×	7	1.4
ibmpg6t	100	53.68	83.41	1.0e-3	2.7e-4	7.9×	13.3×	7	1.4
ibmpg1t_new	100	1.02	1.57	1.0e-3	1.9e-4	4.8×	50.3×	6	1.1
ibmpg2t_new	100	2.27	4.39	1.0e-3	2.1e-4	11.2×	190.1×	6	1.3
ibmpg3t_new	100	27.48	60.34	7.2e-4	1.8e-4	7.1×	135.2×	6	1.4
ibmpg4t_new	15	40.11	82.01	4.4e-4	3.5e-5	2.9×	125.8×	8	1.4
ibmpg5t_new	100	45.56	69.20	9.3e-4	1.9e-4	6.3×	111.2×	7	1.4
ibmpg6t_new	100	62.92	98.57	1.8e-3	2.0e-4	7.3×	111.5×	7	1.4
Average	—	—	—	—	—	7.6×	68.0×	—	—

REFERENCES

- [1] H. Zhuang, S.-H. Weng, J.-H. Lin, and C. K. Cheng, "MATEX: A distributed framework of transient simulation of power distribution networks," in *Proc. IEEE/ACM Design Autom. Conf.*, 2014.
- [2] D. Kouroussis and F. N. Najm, "A static pattern-independent technique for power grid voltage integrity verification," in *Proc. IEEE/ACM Design Autom. Conf.*, pp. 99–104, 2003.
- [3] S. R. Nassif and J. N. Kozhaya, "Fast power grid simulation," in *Proc. IEEE/ACM Design Autom. Conf.*, pp. 156–161, 2000.
- [4] M. S. Gupta, J. L. Oatley, R. Joseph, G.-Y. Wei, and D. M. Brooks, "Understanding voltage variations in chip multiprocessors using a distributed power-delivery network," in *Proc. DATE*, pp. 1–6, 2007.
- [5] S. Lin, M. Nagata, K. Shimazake, K. Satoh, M. Sumita, H. Tsujikawa, and A. T. Yang, "Full-chip vectorless dynamic power integrity analysis and verification against 100uv/100ps-resolution measurement," in *Proc. IEEE CICC*, pp. 509–512, 2004.
- [6] S. Lin and N. Chang, "Challenges in power-ground integrity," in *Proc. IEEE/ACM Int. Conf. Comput.-Aided Design*, pp. 651–654, 2001.
- [7] R. Zhang, B. H. Meyer, W. Huang, K. Skadron, and M. R. Stan, "Some limits of power delivery in the multicore era," *WEED*, 2012.
- [8] R. Zhang, K. Wang, B. H. Meyer, M. R. Stan, and K. Skadron, "Architecture implications of pads as a scarce resource," in *Proc. IEEE/ACM Intl Symp. Computer Architecture*, pp. 373–384, 2014.
- [9] K. Wang, B. H. Meyer, R. Zhang, G. Hu, and M. R. Stan, "Walking pads: Fast power-supply pad-placement optimization," in *Proc. IEEE/ACM Asia South Pac. Design Autom. Conf.*, vol. 20, p. 4, 2014.
- [10] J. Lu, H. Zhuang, P. Chen, H. Chang, C.-C. Chang, Y.-C. Wong, L. Sha, D. Huang, Y. Luo, C.-C. Teng, and C. K. Cheng, "ePlace-MS: Electrostatics based placement for mixed-size circuits," *IEEE Trans. Comput.-Aided Design Integr. Circuits Syst.*, 2015.
- [11] J. Lu, P. Chen, C.-C. Chang, L. Sha, D. Huang, C.-C. Teng, and C.-K. Cheng, "ePlace: Electrostatics based placement using Nesterov's method," in *Proc. IEEE/ACM Design Autom. Conf.*, 2014.
- [12] S. K. Samal, K. Samadi, P. Kamal, Y. Du, and S. K. Lim, "Full chip impact study of power delivery network designs in monolithic 3D ICs," in *Proc. IEEE/ACM Int. Conf. Comput.-Aided Design*, pp. 565–572, 2014.
- [13] H. Zhuang, J. Lu, K. Samadi, Y. Du, and C. K. Cheng, "Performance-driven placement for design of rotation and right arithmetic shifters in monolithic 3D ICs," in *Proc. IEEE Intl. Conf. Communications, Circuits and Systems*, vol. 2, pp. 509–513, 2013.
- [14] C. Zhuo, G. Wilke, R. Chakraborty, A. Aydiner, S. Chakravarty, and W.-K. Shih, "A silicon-validated methodology for power delivery modeling and simulation," in *Proc. IEEE/ACM Int. Conf. Comput.-Aided Design*, pp. 255–262, 2012.
- [15] Z. Zeng, X. Ye, Z. Feng, and P. Li, "Tradeoff analysis and optimization of power delivery networks with on-chip voltage regulation," in *Proc. IEEE/ACM Design Autom. Conf.*, pp. 831–836, 2010.
- [16] H. Zhuang, X. Wang, I. Kang, J.-H. Lin, and C. K. Cheng, "Dynamic analysis of power delivery network with nonlinear components using matrix exponential method," in *IEEE Intl. Symp. EMC&SI*, 2015.
- [17] H. Zhuang, W. Yu, I. Kang, X. Wang, and C. K. Cheng, "An algorithmic framework for efficient large-scale circuit simulation using exponential integrators," in *Proc. IEEE/ACM Design Autom. Conf.*, 2015.
- [18] S. R. Nassif, "Power grid analysis benchmarks," in *Proc. IEEE/ACM Asia South Pac. Design Autom. Conf.*, pp. 376–381, 2008.
- [19] M. Zhao, R. V. Panda, S. S. Sapatnekar, and D. Blaauw, "Hierarchical analysis of power distribution networks," *IEEE Trans. Comput.-Aided Design Integr. Circuits Syst.*, vol. 21, no. 2, pp. 159–168, 2002.
- [20] Z. Li, R. Balasubramanian, F. Liu, and S. Nassif, "2012 tau power grid simulation contest: benchmark suite and results," in *Proc. IEEE/ACM Int. Conf. Comput.-Aided Design*, pp. 643–646, 2012.
- [21] C. Zhuo, H. Gan, and W.-K. Shih, "Early-stage power grid design: Extraction, modeling and optimization," in *Proc. IEEE/ACM Design Autom. Conf.*, pp. 1–6, 2014.
- [22] H. Zhuang, W. Yu, G. Hu, Z. Liu, and Z. Ye, "Fast floating random walk algorithm for multi-dielectric capacitance extraction with numerical characterization of Green's functions," in *Proc. IEEE/ACM Asia South Pac. Design Autom. Conf.*, pp. 377–382, 2012.
- [23] C. Zhang and W. Yu, "Efficient space management techniques for large-scale interconnect capacitance extraction with floating random walks," *IEEE Trans. Comput.-Aided Design Integr. Circuits Syst.*, vol. 32, no. 10, pp. 1633–1637, 2013.
- [24] W. Yu, H. Zhuang, C. Zhang, G. Hu, and Z. Liu, "RWCAP: A floating random walk solver for 3-D capacitance extraction of very-large-scale integration interconnects," *IEEE Trans. Comput.-Aided Design Integr. Circuits Syst.*, vol. 32, no. 3, pp. 353–366, 2013.
- [25] L. O. Chua and P.-M. Lin, *Computer Aided Analysis of Electric Circuits: Algorithms and Computational Techniques*. Prentice-Hall, 1975.
- [26] Y. Saad, *Iterative Methods for Sparse Linear Systems*. SIAM, 2003.
- [27] T. A. Davis, *Direct Method for Sparse Linear Systems*. SIAM, 2006.
- [28] T. Yu and M. D.-F. Wong, "PGT_SOLVER: An efficient solver for power grid transient analysis," in *Proc. IEEE/ACM Int. Conf. Comput.-Aided Design*, pp. 647–652, 2012.
- [29] J. Yang, Z. Li, Y. Cai, and Q. Zhou, "Powerrush: Efficient transient simulation for power grid analysis," in *Proc. IEEE/ACM Int. Conf. Comput.-Aided Design*, pp. 653–659, 2012.
- [30] X. Xiong and J. Wang, "Parallel forward and back substitution for efficient power grid simulation," in *Proc. IEEE/ACM Int. Conf. Comput.-Aided Design*, pp. 660–663, 2012.
- [31] L. Nagel, *SPICE2: A computer program to simulate semiconductor circuits*. Ph.D. dissertation, 1975.
- [32] S.-H. Weng, Q. Chen, and C. K. Cheng, "Time-domain analysis of large-scale circuits by matrix exponential method with adaptive control," *IEEE Trans. Comput.-Aided Design Integr. Circuits Syst.*, vol. 31, no. 8, pp. 1180–1193, 2012.
- [33] Y. Saad, "Analysis of some krylov subspace approximations to the matrix exponential operator," *SIAM J. Numer. Anal.*, vol. 29, no. 1, pp. 209–228, 1992.

- [34] M. Armbrust, A. Fox, R. Griffith, A. D. Joseph, R. Katz, A. Konwinski, G. Lee, D. Patterson, A. Rabkin, I. Stoica, and M. Zaharia, "A view of cloud computing," *Communications of the ACM*, vol. 53, no. 4, pp. 50–58, 2010.
- [35] B. Hindman, A. Konwinski, M. Zaharia, A. Ghodsi, A. D. Joseph, R. Katz, S. Shenker, and I. Stoica, "Mesos: A platform for fine-grained resource sharing in the data center," in *NSDI*, pp. 22–22, 2011.
- [36] J. Dean and S. Ghemawat, "Mapreduce: simplified data processing on large clusters," *CACM*, vol. 51, no. 1, pp. 107–113, 2008.
- [37] M. Zaharia, M. Chowdhury, M. J. Franklin, S. Shenker, and I. Stoica, "Spark: cluster computing with working sets," in *HotCloud*, pp. 10–10, 2010.
- [38] Q. He, W. Au, A. Korobkov, and S. Venkateswaran, "Parallel power grid analysis using distributed direct linear solver," in *IEEE Intl. Symp. EMC*, pp. 866–871, 2014.
- [39] N. Gupte and J. Wang, "Secure power grid simulation on cloud," *IEEE Trans. Comput.-Aided Design Integr. Circuits Syst.*, vol. 34, no. 3, pp. 422–432, 2015.
- [40] J. Wang and X. Xiong, "Scalable power grid transient analysis via mor-assisted time-domain simulations," in *Proc. IEEE/ACM Int. Conf. Comput.-Aided Design*, 2013.
- [41] X.-X. Liu, H. Wang, and S. X.-D. Tan, "Parallel power grid analysis using preconditioned gmres solver on CPU-GPU platforms," in *Proc. IEEE/ACM Int. Conf. Comput.-Aided Design*, pp. 561–568, IEEE, 2013.
- [42] Z. Feng and P. Li, "Multigrid on GPU: tackling power grid analysis on parallel simt platforms," in *Proc. IEEE/ACM Int. Conf. Comput.-Aided Design*, pp. 647–654, 2008.
- [43] S.-H. Weng, Q. Chen, N. Wong, and C. K. Cheng, "Circuit simulation via matrix exponential method for stiffness handling and parallel processing," in *Proc. IEEE/ACM Int. Conf. Comput.-Aided Design*, pp. 407–414, 2012.
- [44] J. van den Eshof and M. Hochbruck, "Preconditioning lanczos approximations to the matrix exponential," *SIAM J. Sci. Comput.*, vol. 27, no. 4, pp. 1438–1457, 2006.
- [45] M. A. Botchev, "A short guide to exponential krylov subspace time integration for maxwell's equations," Dept. of Applied Mathematics, Univ. of Twente, 2012.
- [46] H. Zhuang, S.-H. Weng, and C. K. Cheng, "Power grid simulation using matrix exponential method with rational krylov subspaces," in *Proc. IEEE Intl. Conf. ASIC*, 2013.
- [47] Q. Chen, S.-H. Weng, and C. K. Cheng, "A practical regularization technique for modified nodal analysis in large-scale time-domain circuit simulation," *IEEE Trans. Comput.-Aided Design Integr. Circuits Syst.*, vol. 31, no. 7, pp. 1031–1040, 2012.
- [48] J. Wilkinson, "Kronecker's canonical form and the QZ algorithm," *Linear Algebra and its Applications*, vol. 28, pp. 285–303, 1979.
- [49] P. Li, "Parallel circuit simulation: A historical perspective and recent developments," *Foundations and Trends in Electronic Design Automation*, vol. 5, no. 4, pp. 211–318, 2012.
- [50] X. Ye, M. Zhao, R. Panda, P. Li, and J. Hu, "Accelerating clock mesh simulation using matrix-level macromodels and dynamic time step rounding," in *ISQED*, pp. 627–632, 2008.
- [51] X. Chen, Y. Wang, and H. Yang, "NICSLU: An adaptive sparse matrix solver for parallel circuit simulation," *IEEE Trans. Comput.-Aided Design Integr. Circuits Syst.*, vol. 32, no. 2, pp. 261–274, 2013.
- [52] M. Hochbruck and A. Ostermann, "Exponential integrators," *Acta Numerica*, vol. 19, pp. 209–286, 2010.
- [53] M. Hochbruck, C. Lubich, and H. Selhofer, "Exponential integrators for large systems of differential equations," *SIAM J. Sci. Comput.*, vol. 19, no. 5, pp. 1552–1574, 1998.